ACS APPLIED NANO MATERIALS
Cite This: ACS Appl. Nano Mater. 2018, 1, 1116−1123
Article
www.acsanm.org

Nanocomposites of Oriented Nickel Chains with Tunable Magnetic Properties for High-Performance Broadband Microwave Absorption

Wei Xu,[†] Ya-Fei Pan,[†] Wei Wei,[‡] and Guang-Sheng Wang*[,†,‡]

[†]Key Laboratory of Bio-Inspired Smart Interfacial Science and Technology of Ministry of Education, School of Chemistry, Beihang University, Beijing 100191, P. R. China

[‡]Henan Key Laboratory of Biomolecular Recognition and Sensing, School of Chemistry and Chemical Engineering, Shangqiu Normal University, Shangqiu 476000, P. R. China

Supporting Information

ABSTRACT: Chainlike nickel nanostructures were prepared by using an efficient wet chemical method, and Ni/polyvinylidene fluoride (PVDF) composites were fabricated with a rotational orientation in a static magnetic field. The oriented magnetic nanochains in the composites show a uniform distribution without significant agglomeration, which favors the impedance matching and attenuation ability of the absorbents. The Ni/PVDF composite with only a 20 wt % loading of oriented nickel chains exhibits a minimum reflection loss (RL) value of −36.8 dB at 23.2 GHz from 18 to 26.5 GHz, while an optimal RL of −37.3 dB is obtained at 35.6 GHz with a 10 wt % loading from 26.5 to 40 GHz. Moreover, an excellent electromagnetic interference shielding effectiveness (35 dB) is achieved with an oriented filler loading of 30 wt %. Rotational orientation is an effective strategy for magnetic materials to achieve enhancements in both microwave absorption and shielding performance.

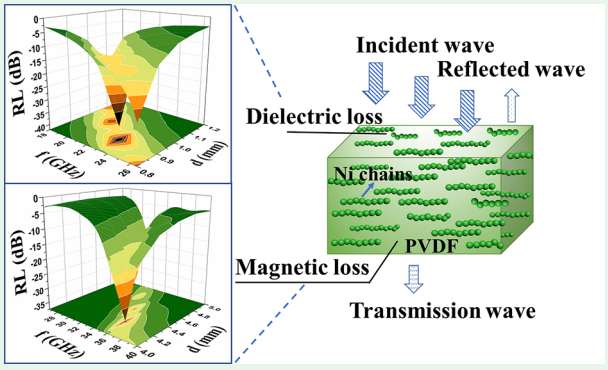

KEYWORDS: *nickel chains, rotational orientation, broadband, microwave absorption, shielding property*

INTRODUCTION

With the swift evolution of information technology, electromagnetic (EM) waves in the range of 2−40 GHz have already been applied to many broadband, multiband, or high-power electronic instruments, such as satellite broadcasting, high-frequency wireless communication, and ultrawide-band radar.[1−3] The use of EM waves with such high frequencies may result in many issues associated with electromagnetic interference (EMI) for electronic equipment, human physical health, and national defense security.[4,5] Generally, there are two practical approaches for solving these potential problems, namely, developing microwave absorption (MA) materials that can effectively eliminate unwanted EM waves over a broadband frequency range and designing EMI shielding materials that act as shields against the penetration of radiation energy.

During the past decade, various materials such as semiconductor nanomaterials, carbon materials, metallic magnets, and their hybrids have been utilized as microwave absorbents and have displayed good performance.[6] As a type of MA material, magnetic materials with large magnetic losses, such as ferrites,[5,7] metals,[8−10] and their alloys[11,12] and compounds,[13] have attracted significant attention. However, there is still the drawback of a narrow absorption frequency due to the Snoek's limit,[14] which restricts the further application of magnetic materials for microwave absorption. To overcome this limitation, tremendous efforts were recently made, and several strategies have been proposed, such as constructing a distinct core@void@shell configuration,[15,16] encapsulating metal in carbon-based materials,[17,18] and other approaches.[19,20] For example, Zhao et al.[21] reported the preparation of Ni@void@SnO_2 composites, and the best microwave absorption property of −50.2 dB was achieved at 17.4 GHz. Zou et al.[22] successfully synthesized composites containing Ni nanowire-filled multiwall carbon nanotubes (MWNTs) and achieved a minimum reflection loss of −23.1 dB at 8.0 GHz. Zhao et al.[23] prepared Ni nanoparticles embedded in porous graphite carbon to form a Ni/carbon foam. The composite reached an effective absorption bandwidth of 4.5 GHz and obtained the minimum reflection value of −45 dB at 13.3 GHz. However, the formation process of this composite was generally quite complicated.

As for EMI shielding materials, many carbon-based materials, including MWNTs, carbon nanocoils (CNCs), graphite nanosheets (GNs), and graphene foam composites used as fillers, have received much attention.[24] For instance, Chen et al.[25] developed graphene/PDMS foam composites with outstanding shielding effectiveness (∼20 dB) and mechanical flexibility. Mural et al.[26] achieved an EMI SE of ∼27 dB for PE/

Received: December 5, 2017
Accepted: February 14, 2018
Published: February 14, 2018

DOI: 10.1021/acsanm.7b00293
ACS Appl. Nano Mater. 2018, 1, 1116−1123

PEO blends containing 3 wt % MWNTs and 52 wt % Ni. Singh et al.[27] employed cobalt/nickel nanoparticles in single-walled carbon nanotubes to form Co/Ni@SWCNT composites, and the product presented a shielding effectiveness value of 24 dB. It is well-known that carbon-based materials can act as efficient EMI shields, and their low percolation threshold, high specific surface area, and large aspect ratios are mostly responsible for their high performance.[1,28] However, such advantages may lead to severe agglomeration that impairs their mechanical properties to a certain extent. In this case, functional fillers were rationally assembled through rotational orientation, demonstrating a novel approach for achieving a homogeneous dispersion and alignment distribution. The EM parameters of the composites can thus be tailored for optimizing performance.

It is widely recognized that EM parameters are crucial factors for the practical applications of microwave absorption and EMI shielding. Recently, rotational orientation to achieve an alignment distribution has become an effective strategy to tune EM parameters, which in turn affects the overall EM wave absorption and shielding efficiency. For instance, Sun and coworkers[29] prepared cross-tacking aligned carbon-nanotube films, which are promising for lightweight, frequency-tunable, and high-performance microwave absorption materials. Li et al.[14] found that orientation could lead to a higher complex permeability that is favorable for achieving an enhanced MA property. Meanwhile, Yousefi et al.[30] demonstrated that a highly aligned graphene/polymer could induce remarkably low percolation and excellent dielectric properties, presenting a high EMI shielding efficiency of 38 dB. However, studies regarding the effect of the filler alignment on microwave absorption and EMI shielding are scarce. Furthermore, most of these studies have been focused on a frequency range of 2−18 GHz, which is much narrower than those of practical applications.

In our previous work, we investigated the MA performance of Ni/polyvinylidene fluoride (PVDF) nanocomposites in the 2−18 GHz range.[31] Here, oriented Ni/PVDF nanocomposites with different Ni proportions were fabricated as microwave absorbents and tested over a wide frequency range of 18−40 GHz for the first time. Significant enhancements in both the absorption intensities and bandwidths were obtained by rotational orientation, and the microwave absorption mechanism was investigated systematically. In addition, the properties of EMI shielding were also studied in detail.

RESULTS AND DISCUSSION

As mentioned in the experimental section, the nickel nanochains were synthesized by a wet chemical method in ethylene glycol. As shown in Figure 1a,b, using only 50 mL of ethylene glycol as a solvent, the products are composed of irregular particles and nanosheets in a disordered aggregate. With increased solvent concentration, the obtained products transform into ball-like spheres with uniform sizes and irregular groove defects on the surface. In the present reaction system, the concentration of hydrazine hydrate acting as both a ligand and a reducing agent is an important factor that influences the growth of nickel nanochains. Figure 1d−f shows a series of scanning electron microscopy (SEM) images of Ni samples with different concentrations of hydrazine hydrate. When the volume of hydrazine hydrate is 0.2 mL, the main products are spheres with rough surfaces and nanosheets, and a certain quantity of spheres is connected to each other to form an orderly chainlike morphology (Figure 1d). Some nanosheets

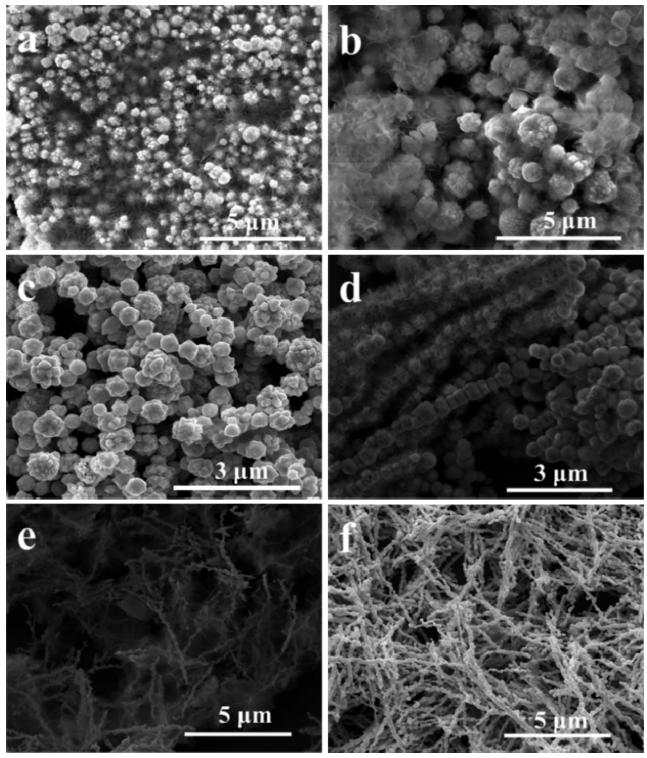

Figure 1. SEM images of nickel samples under different conditions: various concentrations of ethylene glycol (a) and (b) 50 and (c) 100 mL; and various concentrations of hydrazine hydrate (d) 0.2, (e) 0.25, and (f) 0.26 mL.

are formed when 0.25 mL of hydrazine hydrate is used (Figure 1e), and the obtained structures are more like chains. When the volume of the hydrazine hydrate is increased to 0.26 mL, the aggregated nanosheets disappear completely. The products have smoother surfaces, and the nickel chains are longer and more uniform (Figure 1f) with outer diameters and lengths of ∼30 nm and 300 μm, respectively.

A representative bright-field transmission electron microscopy (TEM) image (Figure 2a) suggests a chainlike structure of products with smooth surfaces, and the selected-area electron diffraction (SAED) pattern in Figure 2b shows that the nanochains consist of purely metallic face-centered cubic (fcc) Ni nanoparticles with (111), (200), (220), and (311) planes. These results appear to be consistent with the X-ray diffraction (XRD) result (Figure S1), further illustrating the high purity and cubic structure of the products. Additionally, the cross-sectional SEM images of the samples without and with orientation are shown in Figure 2c,d. In the absence of an external magnetic field, as exhibited in Figure 2c, the nickel nanochains are randomly distributed in the polymer matrix to form disordered chain nets, and some conglomerates in the polymer still exist. When a static magnetic field is applied, homogeneous dispersions of the well-aligned chains are observed in Figure 2d, which indicate that the external magnetic field is sufficiently large to overcome the van der Waals forces between the magnetic chains and drive most of the individual chains into parallel-aligned forms. Moreover, the nickel chains maintain their primary shape in the composites after the hot-press procedure.

A magnetic response in the products is obviously observed when an aqueous suspension of separated nickel chains is held in close proximity to a weak magnet, as shown in Figure S2. All

DOI: 10.1021/acsanm.7b00293
ACS Appl. Nano Mater. 2018, 1, 1116−1123

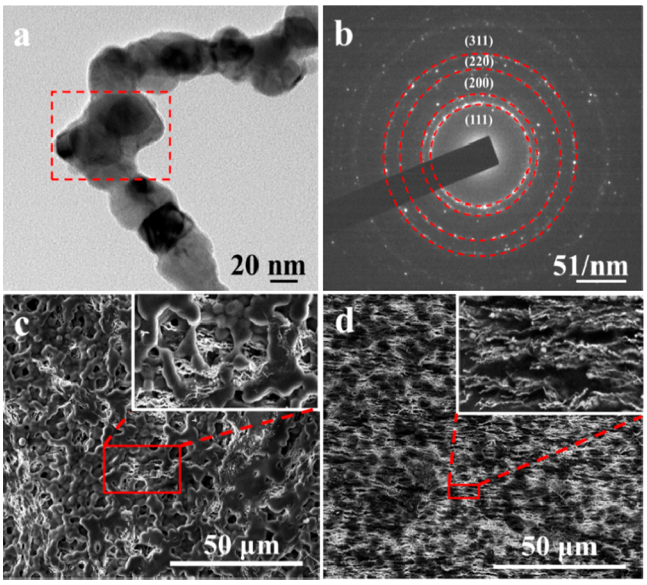

Figure 2. (a) TEM image. (b) Energy-dispersive X-ray spectrum. Cross-sectional SEM images for samples without (c) and with (d) orientation.

products dispersed in deionized water are driven toward the magnetic source in 30 s. The magnetic hysteresis loop is plotted in Figure S2, which expresses typical ferromagnetic behavior. In our previous reports,[31] the effects of magnetic parameters (M_s and H_c) on the microwave absorption performance of the products have been already discussed in detail. At the same time, the magnetic hysteresis loops of unoriented and oriented Ni/PVDF composites are shown in Figure 3. It can be seen that

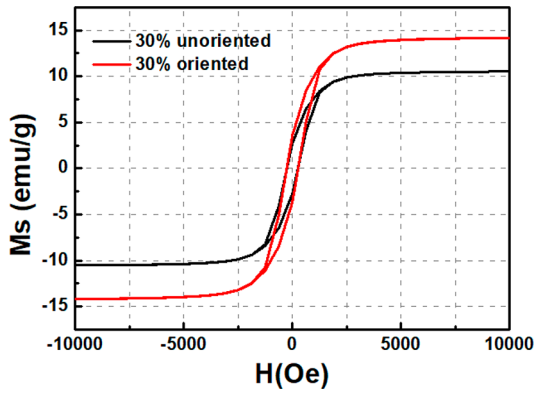

Figure 3. Magnetization hysteresis loop of the oriented and unoriented Ni/PVDF samples.

both of the composites exhibit hysteresis with saturated reversible magnetization, indicating a typical soft ferromagnetic property. In addition, compared with the samples without a rotational orientation, the oriented samples show significantly enhanced magnetism. The increase in magnetism may be ascribed to the improved dispersion of the oriented Ni chains in the matrix. Therefore, it can be concluded that the magnetism of Ni/PVDF can be tuned with the alignment of the nickel chains, which is a key factor to determine their EM properties. Additionally, the results of the contact angle of water on the Ni/PVDF composite show that the oriented samples have larger contact angles than the unoriented samples at different temperatures (Figure S3), demonstrating that the oriented samples have a larger surface energy, which is beneficial for the material to maintain good performance even in a low-temperature environment.

To investigate the effect of the alignment and concentration of Ni chains, various contents of the products have been incorporated into PVDF to fabricate the unoriented and oriented composites. On the basis of transmit-line theory, the microwave absorbing performance of materials is evaluated by the reflection loss (RL) value. On the basis of the measured permittivity and permeability data, the RL value can be obtained using the equation[32,33]

$$\mathrm{RL} = 20 \log \left| \frac{Z_{\mathrm{in}} - 1}{Z_{\mathrm{in}} + 1} \right| \tag{1}$$

Here, Z_{in} is the normalized input characteristic impedance, which can be calculated as follows:

$$Z_{\mathrm{in}} = \sqrt{\frac{\mu_{\mathrm{r}}}{\varepsilon_{\mathrm{r}}}} \tanh\left[j\left(\frac{2f\pi d}{c}\right)\sqrt{\mu_{\mathrm{r}}\varepsilon_{\mathrm{r}}} \right] \tag{2}$$

where ε_{r} ($\varepsilon_{\mathrm{r}} = \varepsilon' - j\varepsilon''$) and μ_{r} ($\mu_{\mathrm{r}} = \mu' - j\mu''$) are the complex permittivity and permeability of the absorbent, respectively; f is the frequency of the EM wave; d is the coating thickness of the absorbent, and c is the velocity of light.

Figure 4 presents the calculated theoretical reflection losses of the two types of samples with different loading contents in the frequency range of 18−26.5 GHz and 26.5−40 GHz. For samples with nickel chains in a random distribution, the RL values are relatively low, and narrow bandwidths with an RL below −10 dB are observed. Nevertheless, the oriented composites show increased reflection losses and effective bandwidths. The results indicate that a minimum RL of −36.8 dB is obtained at 23.2 GHz with a thickness of only 0.9 mm for the 20 wt % nickel nanochains parallelly aligned in the matrix, and the effective absorption bandwidth (RL ≤ 10 dB) is ∼6.5 GHz (Figure 4a), which is comparable to some of the best absorption values ever reported for Ni-nanocomposite materials.[9,17,19,21] Within the range of 26.5−40 GHz, similar phenomena can be observed in Figure 4d. The sample with 10 wt % oriented nickel chains possesses the best microwave absorption, and the minimum RL value reaches −37.3 dB at 35.6 GHz with a thickness of 4.5 mm. Compared with the unoriented composites, both the minimum RL values and the effective absorption bandwidths of the oriented samples are significantly enhanced, which indicates that such an orientation treatment is an effective method to obtain excellent microwave absorption performance.

Figure 4b,c,e,f shows the reflection losses for unoriented and oriented Ni/PVDF composites at various thicknesses with filler loadings of 20 and 10 wt % in the ranges of 18−26.5 and 26.5−40 GHz, respectively. Compared with the samples containing randomly dispersed nickel chains, the oriented samples possess stronger absorption and wider bandwidths with the same loading, further demonstrating that the novel oriented structure has dramatically improved the microwave absorption property. As seen in Figure 4c,f, the RL peaks of the composites shift to low-frequency regions with increasing thickness conforming to the following quarter-wavelength equation[34,35]

$$f_{\mathrm{m}} = \frac{nc}{4t_{\mathrm{m}}\sqrt{|\varepsilon_{\mathrm{r}}||\mu_{\mathrm{r}}|}} (n = 1, 3, 5...) \tag{3}$$

DOI: 10.1021/acsanm.7b00293
ACS Appl. Nano Mater. 2018, 1, 1116−1123

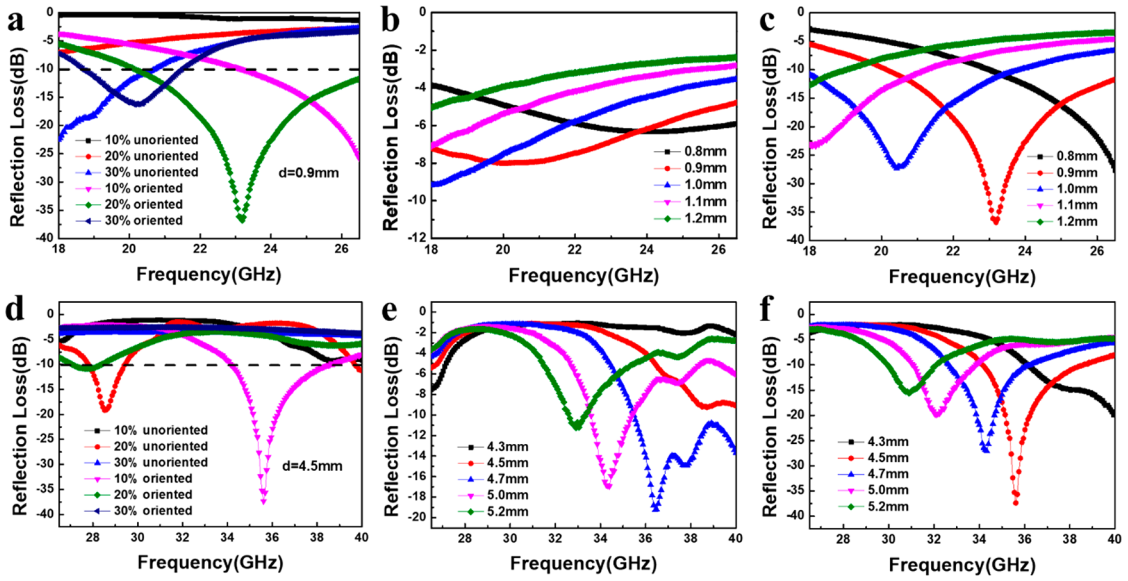

Figure 4. RL curves of (a) the samples with different filler proportions in the frequency range of 18−26.5 GHz; (b) unoriented and (c) oriented Ni/PVDF composites with 20 wt % filler loading. RL curves of (d) the samples with different filler proportions in the frequency range of 26.5−40 GHz; (e) unoriented and (f) oriented Ni/PVDF composites with 10 wt % filler loading.

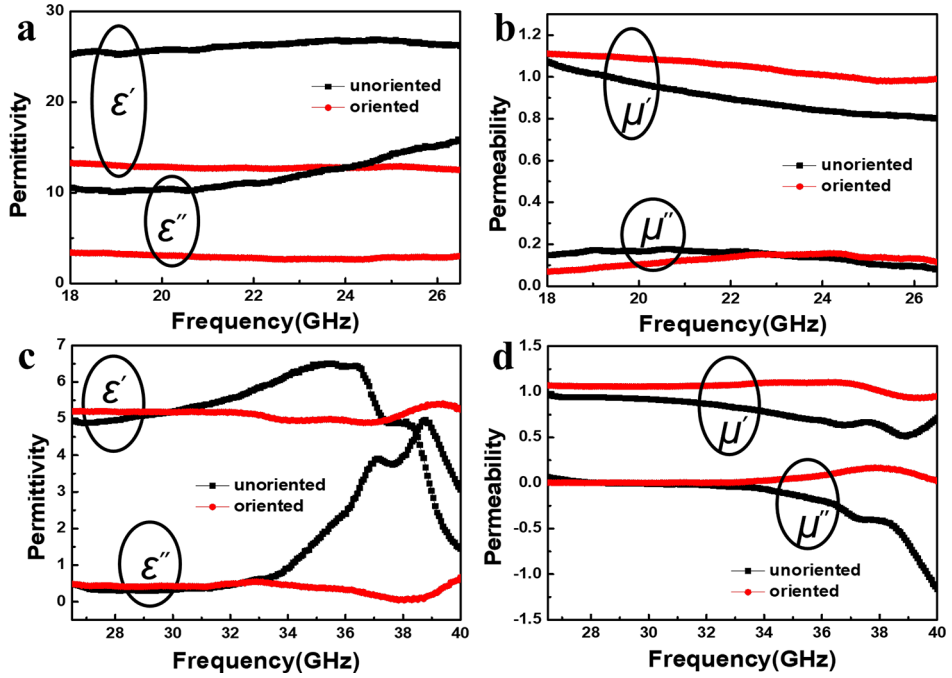

Figure 5. (a) Complex permittivity and (b) complex permeability of the Ni/PVDF samples with a filler loading of 20 wt % from 18 to 26.5 GHz; and (c) complex permittivity and (d) complex permeability of the Ni/PVDF samples with a filler loading of 10 wt % from 26.5 to 40 GHz.

where c is the velocity of light in vacuum, and f_m and t_m represent the matching frequency and thickness of an RL peak, respectively. This relationship illustrates that the microwave absorption behavior can be adjusted by controlling the coating thickness of the absorbents, which is the only way for conventional MA materials to realize frequency regulation. Here, we present an attractive strategy to tune the absorption frequency by controlling the alignment of the fillers. Furthermore, it is worth noting that the oriented samples can achieve −10 dB covering the entire measured frequency range with a thickness from 0.8 to 1.2 mm, which confirms that this type of sample has great potential for a broadband and highly thin microwave absorbent (Figure 4c).

To understand the mechanism for the MA of nickel nanochains with different spatial distributions in the matrix, the complex permittivity and permeability are investigated (Figure 5). The real parts (ε' and μ') stand for the storage abilities of the electric and magnetic energies, and the imaginary parts (ε'' and μ'') represent the inner attenuation capabilities of the electric and magnetic energies, respectively.[36] In a heterogeneous sample composed of fillers and matrix, the ε' values are mainly determined by the interfacial polarization at the interfaces between the metal chains and the insulating

DOI: 10.1021/acsanm.7b00293
ACS Appl. Nano Mater. 2018, 1, 1116−1123

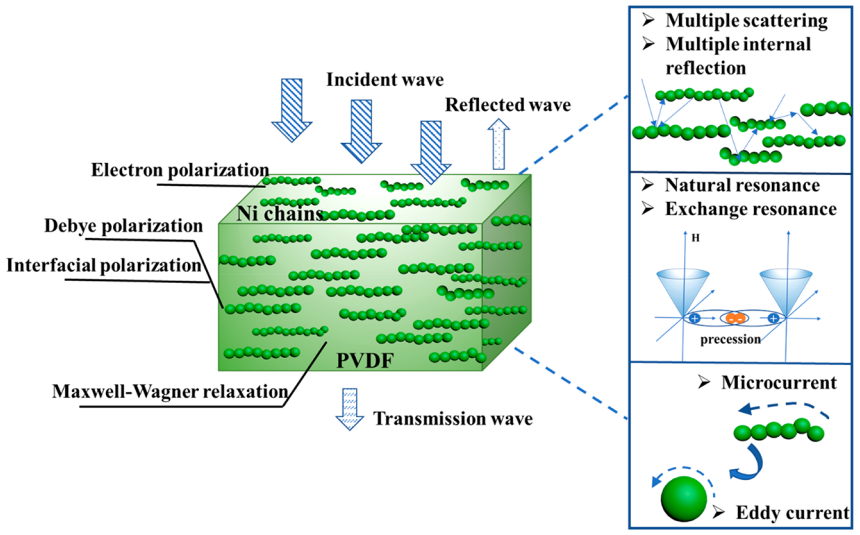

Figure 6. Schematic description of the microwave absorption mechanism for the oriented Ni/PVDF composites.

matrix, and the ε'' values dominantly originate from the conductivity of the metal chain nets. For all the samples, both ε' and ε'' of the oriented samples are slightly smaller than those of the unoriented samples over the entire measured frequency range, resulting from the decreased conductivity of the parallelly oriented nickel chains at low concentrations. However, these lower values favor a balance between permittivity and permeability, leading to a decrease in the reflection coefficient of the absorbents. Hence, benefiting from good impendence matching, the microwave absorption properties of the oriented composites will be improved.

Since Ni is a typical magnetic material, the complex permeability of the composites plays an important role during microwave absorption. In general, all the samples display similar variation trends over the entire frequency range, and under an altering EM field, the items of μ' remain almost constant, indicating the stability of the energy storage capacity. Owing to the rotational orientation, remarkably increased values of μ' and μ'' are observed, which are the decisive factors to promote the MA ability of the samples. The change in μ'' may be attributed to the fact that the planar anisotropy prefers to induce magnetic moments, resulting in the rapid decay of the massive incident EM wave. Meanwhile, note that the values of μ'' of the unoriented samples become negative after 28 GHz, which indicates that the magnetic energy radiates out from the sample.[37] As mentioned above, we can draw a conclusion that both the dielectric loss and magnetic loss are believed to be controlling factors for the achievement of high-performance MA.

To clarify the dielectric behavior based on EM theory, Cole–Cole semicircles of the oriented composites were analyzed. According to Debye's theory, the relative complex permittivity can be expressed by the following equation[38−40]

$$\varepsilon_r = \varepsilon_\infty + \frac{\varepsilon_s - \varepsilon_\infty}{1 + j2\pi f\tau} = \varepsilon' - j\varepsilon'' \tag{4}$$

where f is the frequency, ε_s and ε_∞ are the static permittivity and relative dielectric permittivity at infinite frequency, respectively, and τ is the polarization relaxation time. From eq 4, ε' and ε'' can be described as

$$\varepsilon' = \varepsilon_\infty + \frac{\varepsilon_s - \varepsilon_\infty}{1 + (2\pi f)^2\tau^2} \tag{5}$$

$$\varepsilon'' = \frac{2\pi f\tau(\varepsilon_s - \varepsilon_\infty)}{1 + (2\pi f)^2\tau^2} \tag{6}$$

As inferred from eqs 5 and 6, we can obtain the relationship between ε' and ε''.

$$\left(\varepsilon' - \frac{\varepsilon_s + \varepsilon_\infty}{2}\right)^2 + (\varepsilon'')^2 = \left(\frac{\varepsilon_s - \varepsilon_\infty}{2}\right)^2 \tag{7}$$

On the basis of eq 7, a curve of ε' versus ε'' would form a single semicircle, which is generally denoted as the Cole–Cole semicircle, and each semicircle is associated with one Debye relaxation process. Several Cole–Cole semicircles are clearly observed both in 18–26.5 GHz (Figure S4a) and 26.5–40 GHz (Figure S4b) ranges, indicating that the Debye dielectric relaxation model can account for the permittivity behavior of EM absorbents in the total frequency. However, there are some distortions in the Cole–Cole semicircles, suggesting the probable existence of other polarization loss mechanisms including Maxwell–Wagner relaxation and electron polarization besides the Debye relaxation process.[41]

A magnetic loss analysis of the oriented composites is also conducted. In theory, the magnetic loss mainly arises from magnetic hysteresis, domain wall resonance, eddy current loss, natural resonance, and exchange resonance.[42,43] Magnetic hysteresis only occurs in a strong magnetic field, whereas the domain wall resonance can be negligible because of the nanosized and high-frequency range.[44] The eddy current coefficient can be evaluated by the following equation:[12,45]

$$C_0 = \mu''(\mu')^{-2}f^{-1} = \frac{2}{3}\pi\mu_0 d^2\sigma \tag{8}$$

where μ_0 and σ are the permeability and electrical conductivity of the composites in vacuum, respectively. According to the skin-effect criterion, if magnetic loss only originates from the eddy current loss, the values of C_0 would be constant when the frequency changes.[46] As shown in Figure S4c,d, the values of the C_0 remain approximately constant from 26.5 to 35 GHz and fluctuate in the remaining part of the frequency range, demonstrating that the magnetic loss in the samples is not

DOI: 10.1021/acsanm.7b00293
ACS Appl. Nano Mater. 2018, 1, 1116−1123

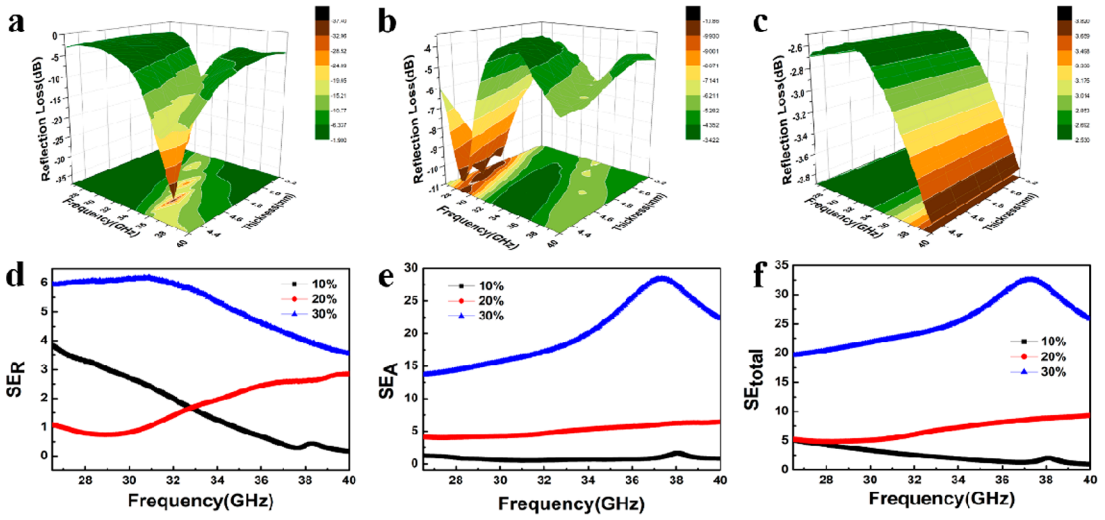

Figure 7. 3D plots of reflection loss for samples with different oriented nickel chain loadings: (a) 10, (b) 20, and (c) 30 wt %. Shielding effectiveness of the (d) reflection, (e) absorption, and (f) total shielding effectiveness of the oriented Ni/PVDF composites from 26.5 to 40 GHz.

only associated with eddy current loss. Hence, the magnetic loss in the measured frequency range is mainly ascribed to the eddy current loss, natural resonance, and exchange resonance. In addition, the decreased particle size and the increased planar anisotropy contribute to a broadening of the natural resonance, which results in more energy dissipation.

Overall, the enhanced MA ability of the oriented sample is attributed to the change in the magnetic loss and the appropriate reduction in the dielectric loss, which are appropriate to meet the requirements of impedance matching. An imagined schematic description is presented in Figure 6, which gives a clear demonstration of the possible MA mechanism. In addition to the magnetic loss that originated from the eddy current, natural resonance, and exchange resonance, the various polarization losses including the Debye relaxation, interfacial relaxation, Maxwell–Wagner relaxation, and electron polarization have significant contributions. Moreover, the structures consisting of parallelly oriented nickel chains contribute to the reflection and refraction by extending the route of incident microwaves and also intensely respond to the broadband microwave absorption.

Finally, the EMI shielding effectiveness (SE) consists of reflected (SE_R), absorbed (SE_A), and multiple (SE_M) reflections and refers to the logarithm of the incident wave P_i to the transmitted wave P_T, which is investigated and calculated by using the measured scattering parameters (S parameters: S_{11}, S_{22}, S_{12}, and S_{21}) as[25,47,48]

$$SE_{total}(dB) = SE_R + SE_A + SE_M = \log_{10}(P_t/P_i) \quad (9)$$

$$SE_R(dB) = 10 \log_{10}(1 - R) \quad (10)$$

$$SE_A(dB) = 10 \log_{10}[T/(1 - R)] \quad (11)$$

In eqs 9, 10, and 11, the power coefficient, reflected power (R), and transmitted power (T) are calculated by the S parameters; that is, $T = |S_{12}|^2 = |S_{21}|^2$, and $R = |S_{11}|^2 = |S_{22}|^2$.[49]

Figure 7 shows the three-dimensional (3D) plots of reflection loss and the shielding performance of the composites filled with 10, 20, and 30 wt % oriented Ni chains in the frequency range of 26.5–40 GHz. The oriented composite with a functional filler content of 10 wt % shows enhanced MA behavior but a relatively low EMI SE value (Figure 7a,f). A lower filling rate results in the poor contact and conductivity, leading to poor shielding performance. In contrast, the composite containing 30 wt % of oriented Ni shows a high EMI shielding effectiveness of 20–35 dB over the entire measured frequency, which reaches the commercial application level (>20 dB).[50] The increment in the EMI SE_{total} is mainly due to the enhanced electrical conductivity (Figure S5). Normally, with an increasing mass ratio, increasingly more conducting interconnections appear, which can promote the EMI shielding performance. These results demonstrate that the oriented Ni/PVDF composites exhibit high performance in microwave absorption at a low filler proportion, whereas the composites with a high mass ratio manifest an outstanding shielding property. Moreover, compared with the unoriented samples (Figure S6), the oriented samples also display enhanced EMI shielding performance, suggesting a highly sufficient contribution of rotational orientation of fillers as well.

CONCLUSIONS

In summary, chainlike nickel nanomaterials were synthesized on a large scale, and oriented Ni/PVDF composites were successfully fabricated by setting an externally applied magnetic field. In systems with oriented nickel chains, the Ni/PVDF composites possessed more induced magnetic moments that resulted in a significant increase in magnetic loss, thus leading to a remarkable improvement in microwave absorption. Within the range of 18–40 GHz, the minimum reflection losses of −36.8 dB at 23.2 GHz and −37.3 dB at 35.6 GHz for the oriented Ni/PVDF nanocomposites (20 and 10 wt %) with thicknesses of 0.9 mm and 4.5 mm were achieved, respectively. Furthermore, the EMI shielding effectiveness of all the samples was measured in the frequency range of 26.5–40 GHz, and an excellent EMI shielding efficiency up to 35 dB was obtained. This method opens a new avenue in designing metal–polymer composites, which can be considered as potential candidates for effective lightweight EM absorption and shielding materials in stealth technology and radar antireflection coatings.

DOI: 10.1021/acsanm.7b00293
ACS Appl. Nano Mater. 2018, 1, 1116–1123

■ ASSOCIATED CONTENT

Supporting Information

The Supporting Information is available free of charge on the ACS Publications website at DOI: 10.1021/acsanm.7b00293.

Experimental details, XRD and magnetization hysteresis loop, photographs of the contact angle of water on the Ni/PVDF composites, curves of ε' versus ε'', C_0–f curves, and EMI shielding performance of the oriented and unoriented Ni/PVDF composites (PDF)

■ AUTHOR INFORMATION

Corresponding Author

*E-mail: wanggsh@buaa.edu.cn.

ORCID

Guang-Sheng Wang: 0000-0002-2408-9260

Notes

The authors declare no competing financial interest.

■ ACKNOWLEDGMENTS

This project was supported by the National Nature Science Foundation of China (No. 51472012) and the Fundamental Research Funds for the Central Universities.

■ REFERENCES

(1) Zhang, Y.; Huang, Y.; Zhang, T. F.; Chang, H. C.; Xiao, P. S.; Chen, H. H.; Huang, Z. Y.; Chen, Y. S. Broadband and Tunable High-Performance Microwave Absorption of an Ultralight and Highly Compressible Graphene Foam. *Adv. Mater.* **2015**, *27*, 2049−53.

(2) Ting, T. H.; Chiang, C. C.; Cheng, K. F.; Hong, Y. S. Effect of Silicon Carbide Dispersion on the Microwave Absorbing Properties of Silicon Carbide-Epoxy Composites in 2−40 GHz. *J. Polym. Res.* **2016**, *23*, 1−5.

(3) Lian, L. X.; Deng, L. J.; Han, M.; Tang, W.; Feng, S. D. Microwave Electromagnetic and Absorption Properties of $Nd_2Fe_{14}B$/α-Fe Nanocomposites in the 0.5−18 and 26.5−40 GHz Ranges. *J. Appl. Phys.* **2007**, *101*, 207.

(4) Egami, Y.; Yamamoto, T.; Suzuki, K.; Yasuhara, T.; Higuchi, E.; Inoue, H. Stacked Polypyrrole-Coated Non-Woven Fabric Sheets for Absorbing Electromagnetic Waves with Extremely High Frequencies. *J. Mater. Sci.* **2012**, *47*, 382−390.

(5) Ohlan, A.; Singh, K.; Chandra, A.; Dhawan, S. K. Microwave Absorption Behavior of Core-Shell Structured Poly(3,4-Ethylenedioxy Thiophene)-Barium Ferrite Nanocomposites. *ACS Appl. Mater. Interfaces* **2010**, *2*, 927−933.

(6) Ran, J.; Shen, L. X.; Zhong, L.; Fu, H. Q. Synthesis of Silanized MoS_2/Reduced Graphene Oxide for Strong Radar Wave Absorption. *Ind. Eng. Chem. Res.* **2017**, *56*, 10667−10677.

(7) Li, Z. W.; Chen, L.; Ong, C. K. Studies of Static and High-Frequency Magnetic Properties for M-Type Ferrite $BaFe_{12-2x}Co_xZr_xO_{19}$. *J. Appl. Phys.* **2002**, *92*, 3902−3907.

(8) Lv, S. Q.; Pan, Y. F.; Yang, P. B.; Wang, G. S. Hybrids of Cobalt Nanochains and Polyvinylidene Fluoride with Enhanced Microwave Absorption Performance. *RSC Adv.* **2016**, *6*, 55546−55551.

(9) Han, D.; Xiao, N.; Hu, H.; Liu, B.; Song, G.; Yan, H. Ultrasmall Superparamagnetic Ni Nanoparticles Embedded in Polyaniline as a Lightweight and Thin Microwave Absorber. *RSC Adv.* **2015**, *5*, 66667−66673.

(10) Zhan, X.; Tang, H.; Du, Y.; Talbi, A.; Zha, J.; He, J. Facile Preparation of Fe Nanochains and Their Electromagnetic Properties. *RSC Adv.* **2013**, *3*, 15966−15970.

(11) Li, X.; Han, X.; Tan, Y.; Xu, P. Preparation and Microwave Absorption Properties of Ni-B Alloy-Coated Fe_3O_4 Particles. *J. Alloys Compd.* **2008**, *464*, 352−356.

(12) Zhao, B.; Zhao, W. Y.; Shao, G.; Fan, B. B.; Zhang, R. Morphology-Control Synthesis of a Core-Shell Structured NiCu Alloy with Tunable Electromagnetic-Wave Absorption Capabilities. *ACS Appl. Mater. Interfaces* **2015**, *7*, 12951−12960.

(13) Deng, J.; Li, S.; Zhou, Y.; Liang, L.; Zhao, B.; Zhang, X.; Zhang, R. Enhancing the Microwave Absorption Properties of Amorphous CoO Nanosheet-Coated Co (Hexagonal and Cubic Phases) through Interfacial Polarizations. *J. Colloid Interface Sci.* **2018**, *509*, 406−413.

(14) Li, R.; Wang, T.; Tan, G. G.; Zuo, W. L.; Wei, J. Q.; Qiao, L.; Li, F. S. Microwave Absorption Properties of Oriented $Pr_2Fe_{17}N_{3-\delta}$, Particles/Paraffin Composite with Planar Anisotropy. *J. Alloys Compd.* **2014**, *586*, 239−243.

(15) Zhao, B.; Guo, X.; Zhao, W.; Deng, J.; Fan, B.; Shao, G.; Bai, Z.; Zhang, R. Facile Synthesis of Yolk-Shell Ni@void@SnO_2(Ni_3Sn_2) Ternary Composites via Galvanic Replacement/Kirkendall Effect and Their Enhanced Microwave Absorption Properties. *Nano Res.* **2017**, *10*, 331−343.

(16) Liu, J.; Cheng, J.; Che, R.; Xu, J.; Liu, M.; Liu, Z. Synthesis and Microwave Absorption Properties of Yolk-Shell Microspheres with Magnetic Iron Oxide Cores and Hierarchical Copper Silicate Shells. *ACS Appl. Mater. Interfaces* **2013**, *5*, 2503−2509.

(17) Wen, F.; Zhang, F.; Liu, Z. Investigation on Microwave Absorption Properties for Multiwalled Carbon Nanotubes/Fe/Co/Ni Nanopowders as Lightweight Absorbers. *J. Phys. Chem. C* **2011**, *115*, 14025−14030.

(18) Zhao, D. L.; Li, X.; Shen, Z. M. Preparation and Electromagnetic and Microwave Absorbing Properties of Fe-Filled Carbon Nanotubes. *J. Alloys Compd.* **2009**, *471*, 457−460.

(19) Deng, J.; Wang, Q.; Zhou, Y.; Zhao, B.; Zhang, R. Facile Design of a ZnO Nanorod-Ni Core-Shell Composite with Dual Peaks to Tune its Microwave Absorption Properties. *RSC Adv.* **2017**, *7*, 15.

(20) Zhang, X.; Ji, G.; Liu, W.; Quan, B.; Liang, X.; Shang, C.; Cheng, Y.; Du, Y. Thermal Conversion of an Fe_3O_4@Metal-Organic Framework: a New Method for an Efficient Fe-Co/Nanoporous Carbon Microwave Absorbing Material. *Nanoscale* **2015**, *7*, 12932−12942.

(21) Zhao, B.; Guo, X. Q.; Zhao, W. Y.; Deng, J. S.; Shao, G.; Fan, B. B.; Bai, Z. Y.; Zhang, R. Yolk-shell Ni@SnO_2 Composites with a Designable Interspace to Improve Electromagnetic Wave Absorption Properties. *ACS Appl. Mater. Interfaces* **2016**, *8*, 28917−28925.

(22) Zou, T. C.; Li, H. P.; Zhao, N. Q.; Shi, C. S. Electromagnetic and Microwave Absorbing Properties of Multi-Walled Carbon Nanotubes Filled with Ni Nanowire. *J. Alloys Compd.* **2010**, *496*, L22−L24.

(23) Zhao, H. B.; Fu, Z. B.; Chen, H. B.; Zhong, M. L.; Wang, C. Y. Excellent Electromagnetic Absorption Capability of Ni/Carbon Based Conductive and Magnetic Foams Synthesized via a Green One Pot Route. *ACS Appl. Mater. Interfaces* **2016**, *8*, 1468−1477.

(24) Wen, B.; Cao, M. S.; Lu, M. M.; Cao, W. Q.; Shi, H. L.; Liu, J.; Wang, X. X.; Jin, H. B.; Fang, X. Y.; Wang, W. Z.; Yuan, J. Reduced Graphene Oxides: Light-Weight and High-Efficiency Electromagnetic Interference Shielding at Elevated Temperatures. *Adv. Mater.* **2014**, *26*, 3484−3489.

(25) Chen, Z.; Xu, C.; Ma, C.; Ren, W.; Cheng, H. M. Lightweight and Flexible Graphene Foam Composites for High-Performance Electromagnetic Interference Shielding. *Adv. Mater.* **2013**, *25*, 1296−1300.

(26) Mural, P. K. S.; Pawar, S. P.; Jayanthi, S.; Madras, G.; Sood, A. K.; Bose, S. Engineering Nanostructures by Decorating Magnetic Nanoparticles onto Graphene Oxide Sheets to Shield Electromagnetic Radiations. *ACS Appl. Mater. Interfaces* **2015**, *7*, 16266−78.

(27) Singh, B. P.; Saket, D. K.; Singh, A. P.; Pati, S.; Gupta, T. K.; Singh, V. N.; Dhakate, S. R.; Dhawan, S. K.; Kotnala, R. K.; Mathur, R. B. Microwave Shielding Properties of Co/Ni Attached to Single Walled Carbon Nanotubes. *J. Mater. Chem. A* **2015**, *3*, 13203−13209.

(28) Guo, A. P.; Zhang, X. J.; Wang, S. W.; Zhu, J. Q.; Yang, L.; Wang, G. S. Excellent Microwave Absorption and Electromagnetic Interference Shielding Based on Reduced Graphene Oxide@MoS_2/Poly(vinylidene fluoride) Composites. *ChemPlusChem* **2016**, *81*, 1305−1311.

DOI: 10.1021/acsanm.7b00293
ACS Appl. Nano Mater. 2018, 1, 1116−1123

(29) Sun, H.; Che, R. C.; You, X.; Jiang, Y. S.; Yang, Z. B.; Deng, J.; Qiu, L. B.; Peng, H. S. Cross-Stacking Aligned Carbon-Nanotube Films to Tune Microwave Absorption Frequencies and Increase Absorption Intensities. *Adv. Mater.* **2014**, *26*, 8120−8125.
(30) Yousefi, N.; Sun, X.; Lin, X.; Shen, X.; Jia, J.; Zhang, B.; Tang, B.; Chan, M.; Kim, J. K. Highly Aligned Graphene/Polymer Nanocomposites with Excellent Dielectric Properties for High Performance Electromagnetic Interference Shielding. *Adv. Mater.* **2014**, *26*, 5480−5487.
(31) Xu, W.; Pan, Y. F.; Wei, W.; Wang, G. S.; Qu, P. Microwave Absorption Enhancement and Dual-nonlinear Magnetic Resonance of Ultrasmall Nickel with Quasi-One-Dimensional Nanostructure. *Appl. Surf. Sci.* **2018**, *428*, 54−60.
(32) Yan, L.; Wang, X.; Zhao, S.; Li, Y.; Gao, Z.; Zhang, B.; Cao, M. S.; Qin, Y. Highly Efficient Microwave Absorption of Magnetic Nanospindle-Conductive Polymer Hybrids by Molecular Layer Deposition. *ACS Appl. Mater. Interfaces* **2017**, *9*, 11116−11125.
(33) Wen, F.; Zhang, F.; Xiang, J.; Hu, W.; Yuan, S.; Liu, Z. Microwave Absorption Properties of Multiwalled Carbon Nanotube/FeNi Nanopowders as Light-Weight Microwave Absorbers. *J. Magn. Magn. Mater.* **2013**, *343*, 281−285.
(34) Wu, T.; Liu, Y.; Zeng, X.; Cui, T. T.; Zhao, Y. T.; Li, Y. N.; Tong, G. X. Facile Hydrothermal Synthesis of Fe_3O_4/C Core-Shell Nanorings for Efficient Low-Frequency Microwave Absorption. *ACS Appl. Mater. Interfaces* **2016**, *8*, 7370.
(35) Feng, Y. B.; Qiu, T. Preparation, Characterization and Microwave Absorbing Properties of FeNi Alloy Prepared by Gas Atomization Method. *J. Alloys Compd.* **2012**, *513*, 455−459.
(36) Zhang, X. J.; Li, S.; Wang, S. W.; Yin, Z. J.; Zhu, J. Q.; Guo, A. P.; Wang, G. S.; Yin, P. G.; Guo, L. Self-Supported Construction of Three-Dimensional MoS_2 Hierarchical Nanospheres with Tunable High-Performance Microwave Absorption in Broadband. *J. Phys. Chem. C* **2016**, *120*, 22019−22027.
(37) Deng, L. J.; Han, M. G. Microwave Absorbing Performances of Multiwalled Carbon Nanotube Composites with Negative Permeability. *Appl. Phys. Lett.* **2007**, *91*, 3119.
(38) Yu, H. L.; Wang, T. S.; Wen, B.; Lu, M. M.; Xu, Z.; Zhu, C. L.; Chen, Y. J.; Xue, X. Y.; Sun, C. W.; Cao, M. S. Graphene/Polyaniline Nanorod Arrays: Synthesis and Excellent Electromagnetic Absorption Properties. *J. Mater. Chem.* **2012**, *22*, 21679−21685.
(39) Jian, X.; Wu, B.; Wei, Y. F.; Dou, S. X.; Wang, X. L.; He, W. D.; Mahmood, N. Facile Synthesis of Fe_3O_4/GCs Composites and Their Enhanced Microwave Absorption Properties. *ACS Appl. Mater. Interfaces* **2016**, *8*, 6101−6109.
(40) Liu, X.; Wang, L. S.; Ma, Y. T.; Zheng, H. F.; Lin, L.; Zhang, Q. F.; Chen, Y. Z.; Qiu, Y. L.; Peng, D. L. Enhanced Microwave Absorption Properties by Tuning Cation Deficiency of Perovskite Oxides of Two-Dimensional $LaFeO_3$/C Composite in X-Band. *ACS Appl. Mater. Interfaces* **2017**, *9*, 7601−7610.
(41) He, S.; Wang, G. S.; Lu, C.; Liu, J.; Wen, B.; Liu, H.; Guo, L.; Cao, M. S. Enhanced Wave Absorption of Nanocomposites Based on the Synthesized Complex Symmetrical CuS Nanostructure and Poly(vinylidene fluoride). *J. Mater. Chem. A* **2013**, *1*, 4685−4692.
(42) Wen, S. L.; Liu, Y.; Zhao, X. C.; Cheng, J. W.; Li, H. Synthesis, Dual-Nonlinear Magnetic Resonance and Microwave Absorption Properties of Nanosheet Hierarchical Cobalt Particles. *Phys. Chem. Chem. Phys.* **2014**, *16*, 18333−18340.
(43) Liu, P.; Huang, Y.; Yan, J.; Yang, Y.; Zhao, Y. Construction of CuS Nanoflakes Vertically Aligned on Magnetically Decorated Graphene and Their Enhanced Microwave Absorption Properties. *ACS Appl. Mater. Interfaces* **2016**, *8*, 5536−5546.
(44) Du, Y.; Liu, W.; Qiang, R.; Wang, Y.; Han, X.; Ma, J.; Xu, P. Shell Thickness-Dependent Microwave Absorption of Core-Shell Fe_3O_4@C Composites. *ACS Appl. Mater. Interfaces* **2014**, *6*, 12997−13006.
(45) Zhao, B.; Shao, G.; Fan, B.; Zhao, W.; Zhang, R. Investigation of the Electromagnetic Absorption Properties of Ni@TiO_2 and Ni@SiO_2 Composite Microspheres with Core-Shell Structure. *Phys. Chem. Chem. Phys.* **2015**, *17*, 2531−2539.
(46) Wu, M.; Zhang, Y. D.; Hui, S.; Xiao, T. D.; Ge, S.; Hines, W. A.; Budnick, J. I.; Taylor, G. W. Microwave Magnetic Properties of $Co_{50}/(SiO_2)_{50}$ Nanoparticles. *Appl. Phys. Lett.* **2002**, *80*, 4404.
(47) Guo, A. P.; Zhang, X. J.; Qu, J. K.; Wang, S. W.; Zhu, J. Q.; Wang, G. S.; Guo, L. Improved Microwave Absorption and Electromagnetic Interference Shielding Properties Based on Graphene-Barium Titanate and Polyvinylidene Fluoride with Varying Content. *Mater. Chem. Front.* **2017**, *1*, 2519−2526.
(48) Wang, J.; Xiang, C.; Liu, Q.; Pan, Y.; Guo, J. Ordered Mesoporous Carbon/Fused Silica Composites. *Adv. Funct. Mater.* **2008**, *18*, 2995−3002.
(49) Maiti, S.; Shrivastava, N. K.; Suin, S.; Khatua, B. B. Polystyrene/MWCNT/Graphite Nanoplate Nanocomposites: Efficient Electromagnetic Interference Shielding Material Through Graphite Nanoplate-MWCNT-Graphite Nanoplate Networking. *ACS Appl. Mater. Interfaces* **2013**, *5*, 4712−4724.
(50) Song, W. L.; Wang, J.; Fan, L. Z.; Li, Y.; Wang, C. Y.; Cao, M. S. Interfacial Engineering of Carbon Nanofiber-Graphene-Carbon Nanofiber Heterojunctions in Flexible Lightweight Electromagnetic Shielding Networks. *ACS Appl. Mater. Interfaces* **2014**, *6*, 10516−10523.

DOI: 10.1021/acsanm.7b00293
ACS Appl. Nano Mater. 2018, 1, 1116−1123